ICAS 2016
30th Congress of the International Council of the Aeronautical Sciences
DCC, Daejeon, Korea ; September 25-30, 2016

NUMERICAL SIMULATION OF DROPLET IMPINGEMENT ON A MULTI-ELEMENT HIGH-LIFT AIRFOIL

L. P. Raj, Ph.D. Candidate, R. S. Myong, Professor
School of Mechanical and Aerospace Engineering and ReCAPT
Gyeongsang National University, Jinju, South Korea

Keywords: *Atmospheric icing, Eulerian, multi-element airfoil, CFD*

Abstract

In this study, a computational method for describing water droplet impingement around a multi-element high-lift airfoil consisting of a slat, main and flap elements is presented. The scheme is developed on the basis of a multi-dimensional unstructured second-order positivity-preserving finite volume upwind method. For the droplet impingement model, the shallow water type droplet model is used as the basic building block for the numerical solver of air-mixed droplet flow. Furthermore, droplet splashing, bouncing, and deformation models were used to take into account the effects of large droplet dynamics on the impingement results. The comparison of the collection efficiency for a multi-element airfoil with experimental result shows good agreement.

1 Introduction

In the Earth's atmosphere, the diluted water droplets can be observed around aircraft flying inside clouds. This issue, called atmospheric in-flight icing, remains as a critical technological issue in the safety of aircraft [1-4]. In this case, determining the impingement area of droplets on solid surfaces is essential in understanding the ice accretion and designing proper ice protection systems (IPS) to prevent (anti-) and remove (de-) ices formed on these surfaces. In particular, information on how efficiently the droplets are collected on the aircraft surface is indispensable to the sizing of an optimized anti-icing system. Detailed knowledge on the location of areas that need protection and the level of external energy consumed are also required in the design of the anti-icing system. These can be obtained using icing wind tunnel tests or CFD simulations. The wind tunnel tests are very expensive in most cases, though they can provide detailed information of droplet impingement area. On the other hand, the state-of-the-art CFD simulations are relatively cheap and can handle icing without suffering scaling issues. The CFD-based simulation methods can be easily utilized for droplet impingement analysis, ice shape prediction, and subsequent performance degradation analysis. As shown in Fig. 1, parameters such as outside air temperature, liquid water content (LWC), median volume diameter (MVD), flight velocity, exposure time, roughness of surface, and shape of the exposed surface are dominant factors affecting the ice accretion.

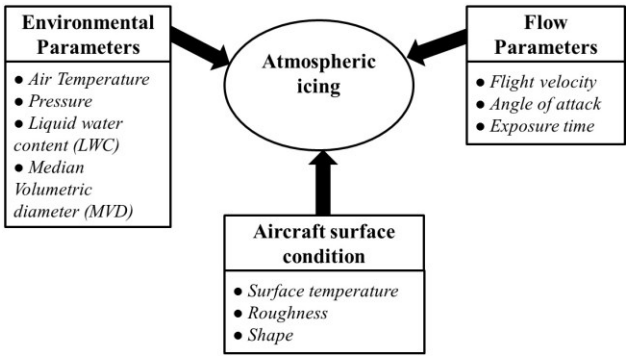

Fig. 1. Factors affecting atmospheric icing

Supercooled large droplets (SLD) are water droplets with a MVD larger than 40 microns. In clouds, these can form through melting of snow or coalescence of smaller droplets under the influence of wind shear. After the fatal crash of an ATR-72 commuter aircraft near Roselawn,

Indiana in 1994, SLD were recognized as extremely hazardous. This type of icing can occur at different locations on the aircraft and is faster and more unpredictable compared to icing by smaller droplets.

According to the current icing regulation, the analysis and design of ice protection system should show that no hazardous quantity of ice forms on the surfaces that are critical for safe operation of the aircraft when exposed to the icing conditions of Appendices C and O [5]. The Appendix O consists of two parts: the first part defines a description of supercooled large drop icing conditions in which the drop median volume diameter (MVD) is less than or greater than 40 μm, the maximum mean effective drop diameter (MED) of Appendix C of this part continuous maximum (stratiform clouds) icing conditions. In this Appendix, supercooled large drop icing conditions consist of freezing drizzle and freezing rain occurring in and/or below stratiform clouds. On the other hand, the second part defines ice accretions used to show compliance with the airplane performance and handling qualities requirements.

In the present work, an Eulerian-based droplet simulation code [3,6] is used for simulating the multi-element airfoil for different flow conditions. For accounting large droplets, semi-empirical formulations are employed to explain the physical properties of droplet deformation and droplet-wall interaction effects. The drag coefficient model is based on the Weber number and the wall interaction model is applied as the numerical boundary condition on the solid surface. Numerical results are compared with the experimental results to verify the applicability of the current computational model for a multi-element airfoil under various meteorological conditions.

2 Governing Equations

The two-phase flows of air-mixed droplet flow can be simulated by a weakly coupled algorithm (one-way coupling) for each of the air and droplet governing equations. This shortcut is possible because the mass loading ratio of the bulk density of the droplets is on the order of 10^{-3} over the bulk density of air in air-droplet flows [7]. The air flow data should then be provided to the droplet solver, through the source terms in the case of the Eulerian droplet equations. The air data around the multi-element airfoil was obtained by a compressible Navier-Stokes code based on a finite volume method using an unstructured mesh topology. In order to employ the turbulent effect, a simple Spalart-Allmaras turbulence model was used.

A shallow water droplet model based on the Eulerian framework developed in the previous work [3] was employed for the present droplet solver, together with the drag deformation and droplet wall interaction models. In the present weakly coupled algorithm, the Eulerian droplet solver is provided with the air flow information computed by the air flow solver through the source term. The shallow water droplet equations are expressed as follows

$$\begin{bmatrix} \rho \\ \rho \mathbf{u} \end{bmatrix}_t + \nabla \cdot \begin{bmatrix} \rho \mathbf{u} \\ \rho \mathbf{u}\mathbf{u} + \rho g MVD \mathbf{I} \end{bmatrix} = \begin{bmatrix} 0 \\ A_{\mathbf{u}}\left(\mathbf{u}_g - \mathbf{u}\right) + \mathbf{S}_b \\ +\nabla \cdot \left(\rho g MVD\right)\mathbf{I} \end{bmatrix}. \quad (1)$$

Here ρ, $\mathbf{u}$, and $\mathbf{u}_g$ are the density of droplets in terms of liquid water content (LWC), and the velocity components of droplet and air, respectively. The *MVD* represents a reference size of droplets. $\boldsymbol{S}_b=\rho g[0, 0, 1-\rho_g/\rho_w]^{\mathrm{T}}$, given by ρ_g and ρ_w as the density of air and water respectively, is the resultant force of the gravity and buoyancy of droplets. The $A_{\mathbf{u}}(\mathbf{u}_g-\mathbf{u})$ denotes the drag on droplets caused by the airflow, and g is acceleration due to gravity. The coefficient $A_{\mathbf{u}}$ can be expressed as

$$\begin{aligned} A_{\mathbf{u}} &= 0.75 \cdot \rho \cdot C_{D_{\mathbf{u}}} \cdot \mathrm{Re}_{\mathbf{u}} \cdot \mu / \rho_w \cdot \mathrm{MVD}^2, \\ \mathrm{Re}_{\mathbf{u}} &= \rho_g \cdot \mathrm{MVD} \cdot \left|\mathbf{u}_g - \mathbf{u}\right| / \mu. \end{aligned} \quad (2)$$

Here μ and MVD are the dynamic viscosity of the gas and the mean volume diameter of the droplet, respectively. $\mathrm{Re}_{\mathbf{u}}$ and $C_{D_{\mathbf{u}}}$ are the Reynolds number of droplets and the drag coefficients of the spherical droplets, respectively. The drag coefficient can be obtained from Lapple [8] as follows

$$C_{D_u} = \frac{24}{\mathrm{Re}_u}\left(1 + 0.0197\,\mathrm{Re}_u^{0.63} + 2.6e^{-4}\cdot \mathrm{Re}_u^{1.38}\right). \quad (3)$$

3 Mathematical Modeling for SLD

The impingement behavior of SLD is different from the conventional droplets. Ice accretion occurs faster and at different locations, hence harder to predict, particularly due to their large size. In order to simulate the large droplets behavior accurately, the original mathematical shallow water droplet model should be extended to include the effects of droplet deformation on the right-hand side of the governing equations. The droplet-wall interactions with droplet trajectories in the vicinity of a solid surface are considered as the numerical boundary condition on the solid surface.

3.1 Drag force

In conventional droplet solvers, it is assumed that the droplet is spherical in shape. But in SLD condition, this assumption is invalid due to the larger size of the droplets. The drag components due to droplet deformation depend on the drag coefficient of the deformed droplet. Large droplets can be stretched and deformed due to the effects of the shear forces and pressure gradients. The degree of deformation can basically be measured by the dimensionless Weber number, We=$\rho_g \cdot V^2 \cdot$MVD/σ, where σ denotes the surface tension of the droplet. The effective droplet drag coefficient is obtained by the interpolation between a sphere and the oblate disk drag coefficient depending on the value of the eccentricity *e,* which can be given as,

$$C_{D_{droplet}} = C_{D_{Sphere}} + e\left(C_{D_{Disk}} - C_{D_{Sphere}}\right). \quad (4)$$

where, $e = 1 - \left(1 + 0.07\ (We)^{0.5}\right)^{-6}$. The droplet behaves as a sphere at low Weber numbers, while it is closer to an oblate disk at higher Weber numbers. The drag coefficients of the sphere and the oblate disk can be summarized for different Reynolds numbers [9]

$$C_{D_{Disk}} = \begin{cases} (64/\pi\,\mathrm{Re})\left[1 + (\mathrm{Re}/2\pi)\right] & \text{if} \quad \mathrm{Re} \le 1.0\text{e-}02, \\ (64/\pi\,\mathrm{Re})\left[1 + 10^{x}\right] & \text{if} \quad 1.0\text{e-}02 < \mathrm{Re} \le 1.5\text{e+}00, \\ (64/\pi\,\mathrm{Re})\left[1 + 0.138\,\mathrm{Re}^{0.792}\right] & \text{if} \quad 1.5\text{e+}00 < \mathrm{Re} \le 1.33\text{e+}02, \\ 1.17 & \text{if} \quad 1.33\text{e+}02 \le \mathrm{Re}. \end{cases} \quad (5)$$

$$C_{D_{Sphere}} = \begin{cases} 0.1875 + 24/\mathrm{Re} & \text{if} \quad \mathrm{Re} < 1.0\text{e-}02, \\ 24\left(1 + 0.1315\,\mathrm{Re}^{(0.82 - 0.05w)}\right)/\mathrm{Re} & \text{if} \quad 1.0\text{e-}02 < \mathrm{Re} \le 2.0\text{e+}01, \\ 24\left(1 + 0.1935\,\mathrm{Re}^{0.6305}\right)/\mathrm{Re} & \text{if} \quad 2.0\text{e+}01 \le \mathrm{Re} \le 2.6\text{e+}02, \\ 10^{\left(1.6435 - 1.1242w + 0.1558w^2\right)} & \text{if} \quad 2.6\text{e+}02 \le \mathrm{Re} \le 1.5\text{e}+03, \\ 10^{\left(-2.4571 + 2.5558w - 0.9295w^2 + 0.1049w^3\right)} & \text{if} \quad 1.5\text{e}+03 \le \mathrm{Re} \le 1.2\text{e}+04, \\ 10^{\left(-1.9181 + 0.6370w - 0.0636w^2\right)} & \text{if} \quad 1.2\text{e}+04 < \mathrm{Re} \le 4.4\text{e}+04, \\ 10^{\left(-4.3390 + 1.5809w - 0.1546w^2\right)} & \text{if} \quad 4.4\text{e}+04 < \mathrm{Re} \le 3.38\text{e}+05, \\ 29.78 - 5.3w & \text{if} \quad 3.38\text{e}+05 < \mathrm{Re} \le 4.0\text{e}+05, \\ 0.1w - 0.49 & \text{if} \quad 4.0\text{e}+05 < \mathrm{Re} \le 1.0\text{e}+06, \\ 0.19 - 8\times10^{4}/\mathrm{Re} & \text{if} \quad 1.0\text{e}+06 < \mathrm{Re}. \end{cases} \quad (6)$$

where $x = -0.883 + 0.906\log_{10}\mathrm{Re} - 0.025(\log_{10}\mathrm{Re})^2$ and $w = \log_{10}\mathrm{Re}$.

3.2 Droplet wall impact model

For the droplet wall impact investigation, many models are applicable for in-flight icing conditions. In the present study, the droplet impact phenomena are divided into four regimes termed as stick, rebound, spread, and splash, using Bai *et al.* [10] model. According to the model, the regimes are specified depending on the Weber number and Laplace number. The regimes can be divided as follows,

$$\begin{cases} f_m = f_u = 0 & \text{if} \quad We \le 2, \\ f_m = 1,\ f_u = f_{\mathrm{V}}^{Bound} & \text{if} \quad 2 < We \le 10, \\ f_m = f_u = 0 & \text{if} \quad 10 < We \le 1320\mathrm{La}^{-0.183}, \\ f_m = f_m^{Splash},\ f_u = f_{\mathrm{V}}^{Splash} & \text{if} \quad We \le 1320\mathrm{La}^{-0.183}. \end{cases} \quad (7)$$

where f_m is the ratio of incoming-to-ejected mass at the solid wall. The splashing model proposed by Trujillo *et al.* [11] is used to determine f_m and it can be expressed as,

$$f_m = \frac{3.8}{\sqrt{f^{*-0.375}\cdot K^{0.5}}}\left\{1 - \exp\left[-f^{*-0.375}\left(K^{0.5} - K_{C_{ir}}^{-0.3125}\right)\right]\right\} \quad (8)$$

where,

$$K = \left(\rho_p^3 MVD^3 V_{np}^5 / \sigma_p^2 \mu_p\right)^{0.25}, \qquad K_{C_{ir}} = 540\left(Rs/MVD\right)^{-0.35}. \quad (9)$$

Here *Rs* [12] represents the maximum surface roughness height, and *f** is the dimensionless droplet frequency written as $1.5(LWC/MVD)^{1/3}$. The secondary velocity of an ejected droplet is based on the rebound and splash factor accounted by Bai *et al.* The adopted equations of motion pertaining to a solid particle rebounding off a solid surface are:

$$u_{t,s} = \frac{5}{7}u_{t,0},$$
$$u_{n,s} = -u_{n,0}\left[0.9930 - 0.0307\left(90^0 - \theta^0\right) + 0.0272\left(90^0 - \theta^0\right)^2 - 0.0086\left(90^0 - \theta^0\right)^3\right]. \quad (10)$$

Here $u_{t,s}$, $u_{n,s}$ are tangential and normal velocity components of post impact velocities. In addition, $u_{n,0}$, $u_{t,0}$ are normal and tangential velocity component of impact velocity of droplets, θ_0 is the angle of incidence of droplet.

3.3 Wall boundary condition

Careful attention must be paid to the implementation of boundary conditions. The droplet impingent is controlled by the projection of normal vector on the solid surface and the droplet velocity in the adjacent cell of the respective solid surface. If the projection is positive, the droplets should not collide with the solid surface. On the other hand, the droplets should collide when the projection is negative. For non-SLD droplets, the solid surface can be given as follows [3],

$$\mathbf{U}_{wall} = 0 \quad \text{if} \quad \mathbf{V}\cdot\mathbf{n} \geq 0,$$
$$\mathbf{U}_{wall} = \mathbf{U} \quad \text{if} \quad \mathbf{V}\cdot\mathbf{n} \leq 0. \quad (11)$$

But in SLD case, splash and rebound property of droplets restrict the use of the above equation. Hence, the boundary conditions for including SLD effects is given as [6],

$$\rho_{wall} = (1 - f_m)\rho_{in}, \; \boldsymbol{U}_{wall} = \boldsymbol{V}_S, \quad \text{if} \quad \mathbf{V}\cdot\mathbf{n} \leq 0. \quad (12)$$

where ρ_{in} is the volume fraction at an adjacent point of the wall, and $\boldsymbol{V}_s$ is the secondary velocity. Since the correlations are done in Lagrangian frame, the quantities are needed to be transferred to global coordinates.

4 Results

An important non-dimensional parameter affecting the ice accretion is the local collection efficiency $\beta = -\alpha\,\mathbf{u}\cdot\mathbf{n}\cdot\beta_{collector}$ where $\beta_{collector}$ is a constant dependent of diameter of the droplets [13].

The experimental collection efficiency data pertaining to the specified droplet impingement has originated from a study performed by Papadakis *et al.* [13] at NASA Glenn's Icing Research tunnel (IRT). The landing configuration of three-element airfoil with slat deflection of 30^0 and flap deflection of 30^0 is used for the icing study. The numerical simulations of ice accretion are performed under the geometric, aerodynamic, and meteorological conditions shown in Table 1.

	Case 1	Case 2	Case 3	Case 4
V(m/s)	76.0	76.0	76.0	76.0
T(K)	276.2	276.2	276.2	276.2
LWC(g/m^3)	0.15	0.15	0.19	0.19
MVD(m)	21.0	21.0	92.0	92.0
α (deg)	0	4	0	4

Table 1. Meteorological conditions

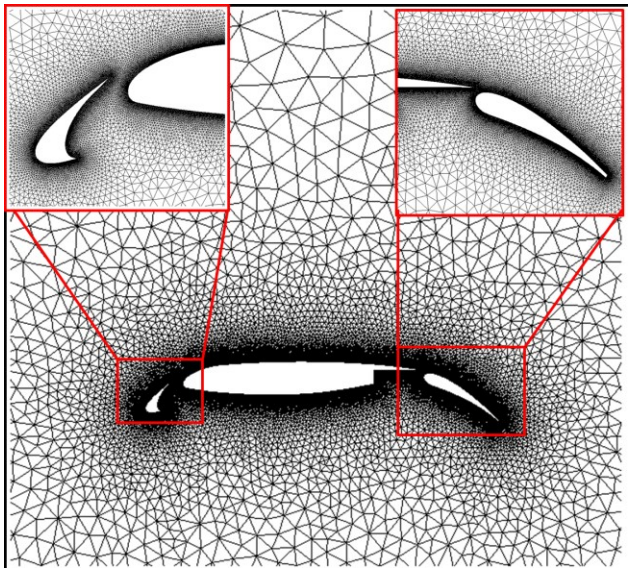

Fig. 2. Unstructured mesh around a three-element airfoil

Fig. 2 shows the unstructured mesh distribution with approximately 55,000 nodes and 95,000 triangular elements around the three-element airfoil. For clean air, a non-slip condition for the wall and the Riemann invariant for far-field boundary condition are employed.

In weakly coupled droplet solvers, the accuracy of droplet solution is mostly depending on the airflow solution and so it is important to validate the airflow solution. Fig. 3 shows the pressure coefficient on a three-element airfoil for 0 degree angle of attack.

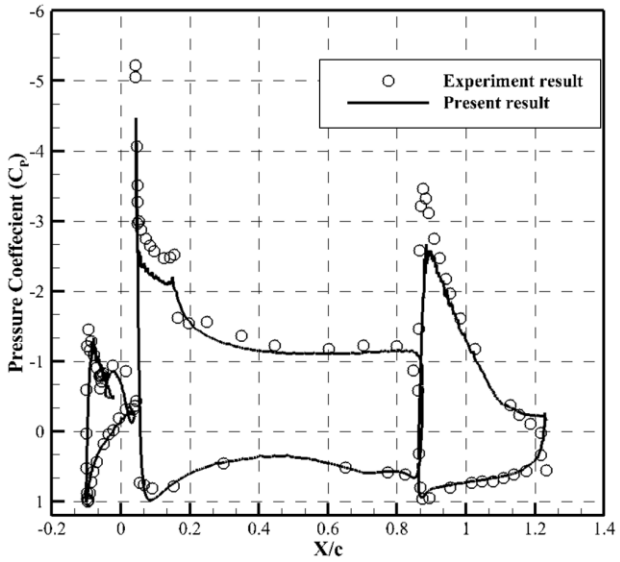

Fig. 3. Experimental and computational results ($\alpha = 0^o$, M = 0.23, Re = 4.9 million)

Fig. 4 depicts the LWC distribution and velocity vector of droplets around the multi-element airfoil for case 2 meteorological condition.

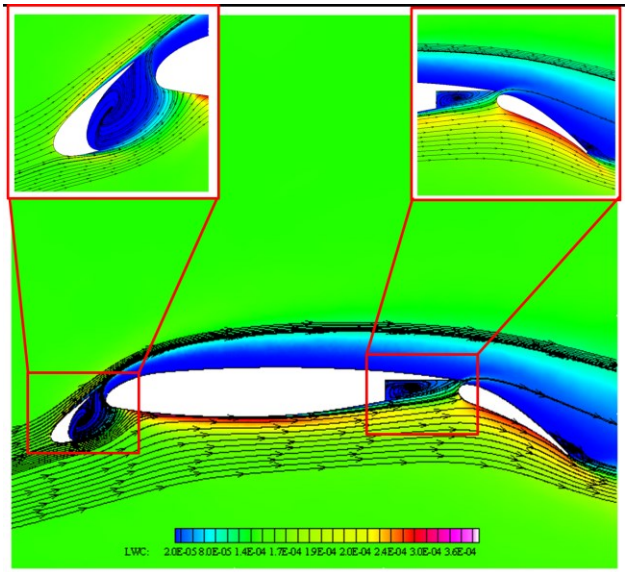

Fig. 4. Liquid water content distribution around the airfoil for case 2.

Near the upper side, cove region of slat, and cove region of main-element, a shadow region area appears signifying a very low density of the LWC. The larger shadow area around the upper side of the model is due to the effect of the free stream angle of attack. The shadow regions indicate that the droplets impingement does not occur on the surface except specified area of the model. Generally, at zero degree angle of attack, the impingements of droplets are higher on the leading edge of slat followed by lower side of the flap. Due to the position of leading edge slat, main-element does not acquire significant impingements at zero degree angle of attack (cases 1 and 3).

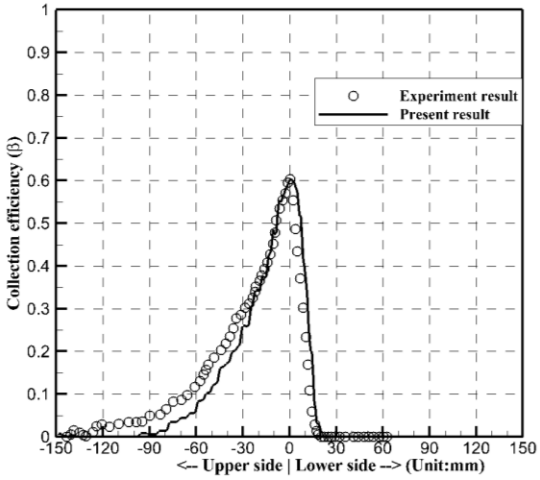

(a)

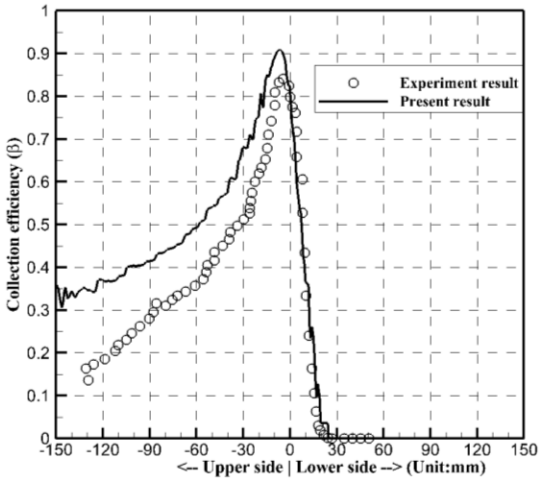

(b)

Fig. 5. Comparison of collection efficiency on the slat for cases 1 and 4.

Fig. 5(a) and 5(b) illustrate the collection efficiency distributions on the slat for cases 1

and 4. As seen in Fig. 5(a) and 5(b), the collection efficiency is increasing with droplet diameter. Also, the impingement area is higher in case 4, which indicates that the droplets diameter is directly affecting the impingement area. These properties have to be taken into account during the design of ice protection systems. Overall, the present computational results show good agreement with the experiment results. However, there are some discrepancies which are easily notable in the impingement area. These gaps may be due to the mono-dispersed assumption of the current computational model which can be minimized by using multi-dispersed droplet distribution. In SLD cases, the collection efficiency is generally over-predicted, which renders a room for improvement in the SLD modeling.

5 Conclusions

In the present study, the droplet impingement over a three-element airfoil is investigated. A CFD code based on an Eulerian-based shallow water droplet model, including the droplet wall interactions and droplet drag model for large droplets, are employed. The computational results are in fairly good agreement with experimental data at given regimes of droplet diameter. However, an improvement of SLD model implementation is necessary for better accuracy. In future, aerodynamic effects of ice accreted multi-element airfoils will be investigated.

Contact Author Email Address

myong@gnu.ac.kr

Acknowledgements

This work was supported by the National Research Foundation of Korea (grant number NRF 2015-M1A3A3A02-010621) through Research Center for Aircraft Parts Technology.

References

[1] Gent RW, Dart NP, Cansdale JT. Aircraft icing. *Philosophical Transactions of the Royal Society of London A: Mathematical, Physical and Engineering Sciences*, Vol. 358, pp 2873-911, 2000.

[2] Kind R, Potapczuk M, Feo A, Golia C, Shah A. Experimental and computational simulation of in-flight icing phenomena. *Progress in Aerospace Sciences*, Vol. 34, pp 257-345, 1998.

[3] Jung SK, Myong RS. A second-order positivity-preserving finite volume upwind scheme for air-mixed droplet flow in atmospheric icing. *Computers & Fluids*, Vol. 86, pp 459-69, 2013.

[4] Ahn GB, Jung KY, Myong RS, Shin HB, Habashi WG. Numerical and experimental investigation of ice accretion on rotorcraft engine air intake. *Journal of Aircraft*, Vol. 52, pp 903-909, 2015.

[5] Parent O, Ilinca A. Anti-icing and de-icing techniques for wind turbines: Critical review. *Cold Regions Science and Technology*, Vol. 65, pp 88-96, 2011.

[6] Jung SK, Myong RS. Numerical modeling for Eulerian droplet impingement in supercooled large droplet conditions. *AIAA Paper 2013-0244*, 2013.

[7] Bourgault Y, Boutanios Z, Habashi WG. Three-dimensional Eulerian approach to droplet impingement simulation using FENSAP-ICE, Part 1: Model, algorithm, and validation. *Journal of Aircraft*, Vol. 37, pp 95-103, 2000.

[8] Lapple C. *Fluid and Particle Mechanics*, Vincent Press, 2007.

[9] Cliff R, Grace J, Weber M. *Bubbles, Drops and Particles*, Academic Press, New York, 1978.

[10] Bai C, Gosman A. Development of methodology for spray impingement simulation. *SAE Technical Paper 950283*, 1995.

[11] Trujillo M, Mathews W, Lee C, Peters J. Modelling and experiment of impingement and atomization of a liquid spray on a wall. *International Journal of Engine Research*, Vol. 1, pp 87-105, 2000.

[12] Honsek R, Habashi WG, Aubé MS. Eulerian modeling of in-flight icing due to supercooled large droplets. *Journal of aircraft*, Vol. 45, pp 1290-1296, 2008.

[13] Papadakis M, Hung KE, Vu GT, Yeong HW, Bidwell CS, Breer MD, Bencic TJ. Experimental investigation of water droplet impingement on airfoils, finite wings, and an S-duct engine inlet. *NASA TM-2002-211700*, 2002.